

# Long term decline of the planktonic biomass in a hotspot of nitrogen fixation

Received: 18 April 2025

Accepted: 13 November 2025

Published online: 28 November 2025

 Check for updates

Alain Fumenia <sup>1</sup>✉, Hubert Loisel<sup>1</sup>, David M. Karl <sup>2</sup>, Vincent Vantrepotte<sup>1</sup>, Anne Petrenko <sup>3</sup>, Sophie Bonnet <sup>3</sup>, Manh Tran-Duy<sup>1</sup>, Marine Bretagnon<sup>4</sup>, Antoine Mangin<sup>4</sup> & Thierry Moutin <sup>3</sup>

Oceanic N<sub>2</sub> fixation by diazotrophic microorganisms is the primary external source of new nitrogen to the surface ocean sustaining net production of organic matter. Studying long-term trends in biomass within N<sub>2</sub> fixation hotspots is crucial for understanding and predicting the response of N<sub>2</sub> fixation to global climate change. Here we developed a bio-optical model based on the spectral phytoplankton absorption coefficient derived from satellite ocean color observations to estimate a proxy for particulate organic nitrogen in the western tropical South Pacific. We demonstrate the existence of a seasonal new biomass production annually over the past 20 years, likely driven by recurrent N<sub>2</sub> fixation. Importantly, our results also reveal a gradual decline in biomass within this N<sub>2</sub> fixation hotspot over the last two decades. This decline indicates that seasonal nitrogen inputs via N<sub>2</sub> fixation are decreasing. This trend inevitably could lead to a decline in the efficiency of the biological carbon pump, with potential implications for global biogeochemical cycles and climate regulation.

The nutrient availability in the upper ocean, and more particularly fixed nitrogen (N) availability<sup>1–3</sup> is a key factor limiting the growth of marine biota and the build-up of organic matter in the ocean<sup>4</sup>. Accordingly, the addition of new N to the bioavailable pool enhances the ocean's capacity to store organic carbon and its derivatives, while removing it might decrease this capacity<sup>4</sup>. The major external source of new N to the surface open ocean, before atmospheric deposition and riverine inputs, is from biological N<sub>2</sub> fixation by diazotrophic microorganisms<sup>5,6</sup>. This process offers the marine phytoplankton community a mechanism to relieve N limitation in the euphotic surface layer, sustaining net production of organic matter in surface waters as well as carbon export from the upper surface to the ocean interior by biological processes (the biological carbon pump, BCP)<sup>7,8</sup>.

The western tropical South Pacific is an oligotrophic area<sup>9</sup>, characterized by an archipelago of islands (referred as the Melanesian archipelago), including New Caledonia, Vanuatu, and Fiji,

situated in the western part of the Tonga-Kermadec subduction zone. Large blooms of diazotrophs have been observed in this vast region extending from the Melanesian archipelago to the Tonga Trench<sup>10–13</sup>. In this area identified as a hotspot of N<sub>2</sub> fixation<sup>14</sup>, previous studies have shown that the net production of organic matter is supported almost exclusively by N<sub>2</sub> fixation, which is primarily controlled by phosphate availability<sup>15</sup> in this iron-rich environment fertilized by the volcanic arc of Tonga<sup>16</sup>. Obtaining an insight into the controls and variability of the particulate organic matter pool produced via N<sub>2</sub> fixation over long temporal scales is thus important for understanding the future role of these parts of ocean as a sink of CO<sub>2</sub>. This is particularly important as the intensity of N<sub>2</sub> fixation, and the amount of particulate organic matter produced and exported may be altered in the future ocean<sup>17–19</sup>. However, despite decades of satellite observations of surface mass concentrations of particulate organic carbon (POC) and chlorophyll-a<sup>20–23</sup>, the temporal and spatial

<sup>1</sup>Laboratoire d'Océanologie et de Géosciences, Université du Littoral Côte d'Opale, Université Lille, CNRS, IRD, UMR 8187, LOG, Wimereux, France. <sup>2</sup>Daniel K. Inouye Center for Microbial Oceanography: Research and Education, University of Hawai'i at Mānoa, Honolulu 96822, USA. <sup>3</sup>Aix Marseille Université, CNRS, Université de Toulon, IRD, OSU Pythéas, Mediterranean Institute of Oceanography (MIO), UM 110, 13288 Marseille, France. <sup>4</sup>ACRI-ST, Sophia Antipolis Cedex 06904, France. ✉e-mail: [alain.fumenia@univ-littoral.fr](mailto:alain.fumenia@univ-littoral.fr)

variability of biomass in the western tropical South Pacific remains poorly characterized.

The use of the seawater inherent optical properties (IOPs) measured in situ or estimated from spaceborne remote-sensing platforms using ocean color radiometry, represents an alternative to discrete measurements of particulate organic matter. To a first order, the variability in particulate IOPs is driven by the total concentration of suspended particulate matter and by composition and particle size distribution at second order. In the western tropical South Pacific, a relationship was identified, for the first time, between surface mass concentrations of particulate organic nitrogen (PON) and spectral particulate backscattering coefficients,  $b_{bp}(\lambda)$ , measurements (where  $\lambda$  is the wavelength in a vacuum) performed by BGC-Argo floats<sup>24</sup>. The use of this relationship made it possible to study the temporal variability of PON and thus to highlight the seasonal increase of biomass during summer periods in absence of significant N sources other than  $N_2$  fixation. However, while BGC-Argo float measurements successfully revealed seasonal-scale variations in PON, they were limited in providing a long-term perspective, which is crucial for understanding the future role of  $N_2$  fixation hotspots. Moreover, although it has been confirmed that  $b_{bp}(\lambda)$  can provide a good proxy of PON in open-ocean environments<sup>24,25</sup>, it has been shown that the total particulate,  $a_p(\lambda)$ , and phytoplankton,  $a_{ph}(\lambda)$ , spectral absorption coefficients demonstrate a better capacity to serve as proxy for PON<sup>25</sup>. The use of satellite ocean color observations currently offers the opportunity to observe trends over relatively long timescales. Given that the IOPs can now be estimated from satellite ocean color observations<sup>26,27</sup>, the use of IOPs estimated from satellite observations therefore offers the unique opportunity to study the spatial and temporal variability of PON over the entire period of satellite data acquisition in environments characterized by active biological  $N_2$  fixation, where N budgets are needed.

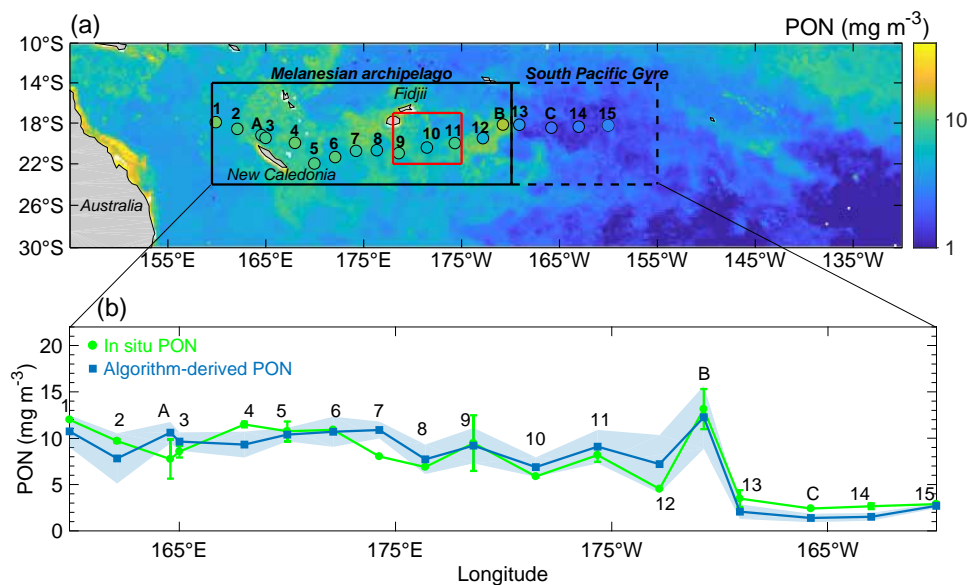
In this study, we aim to assess the seasonal and interannual variability, as well as the trend of PON in the western tropical South Pacific using ocean color remote-sensing data collected from December 2002 to December 2022. To address this, we developed and vali-

dated a new bio-optical model based on  $a_{ph}(\lambda)$  coefficients derived from satellite ocean color observations to estimate PON<sup>26,27</sup>. This algorithm is based on a relationship developed over a global dataset of coincidence between in situ PON measurements and satellite derived  $a_{ph}(\lambda)$  product using the GlobColour<sup>28</sup> remote sensing reflectance as input parameter. The seasonal and interannual variability of PON was analyzed by temporally decomposing the algorithm-derived PON time series using the Census X-11 method<sup>29</sup>. To examine the long-term trend, we applied the non-parametric seasonal Kendall test<sup>29</sup>. Finally, we evaluated the implications of PON concentration temporal trends for the BCP.

## Results and discussion

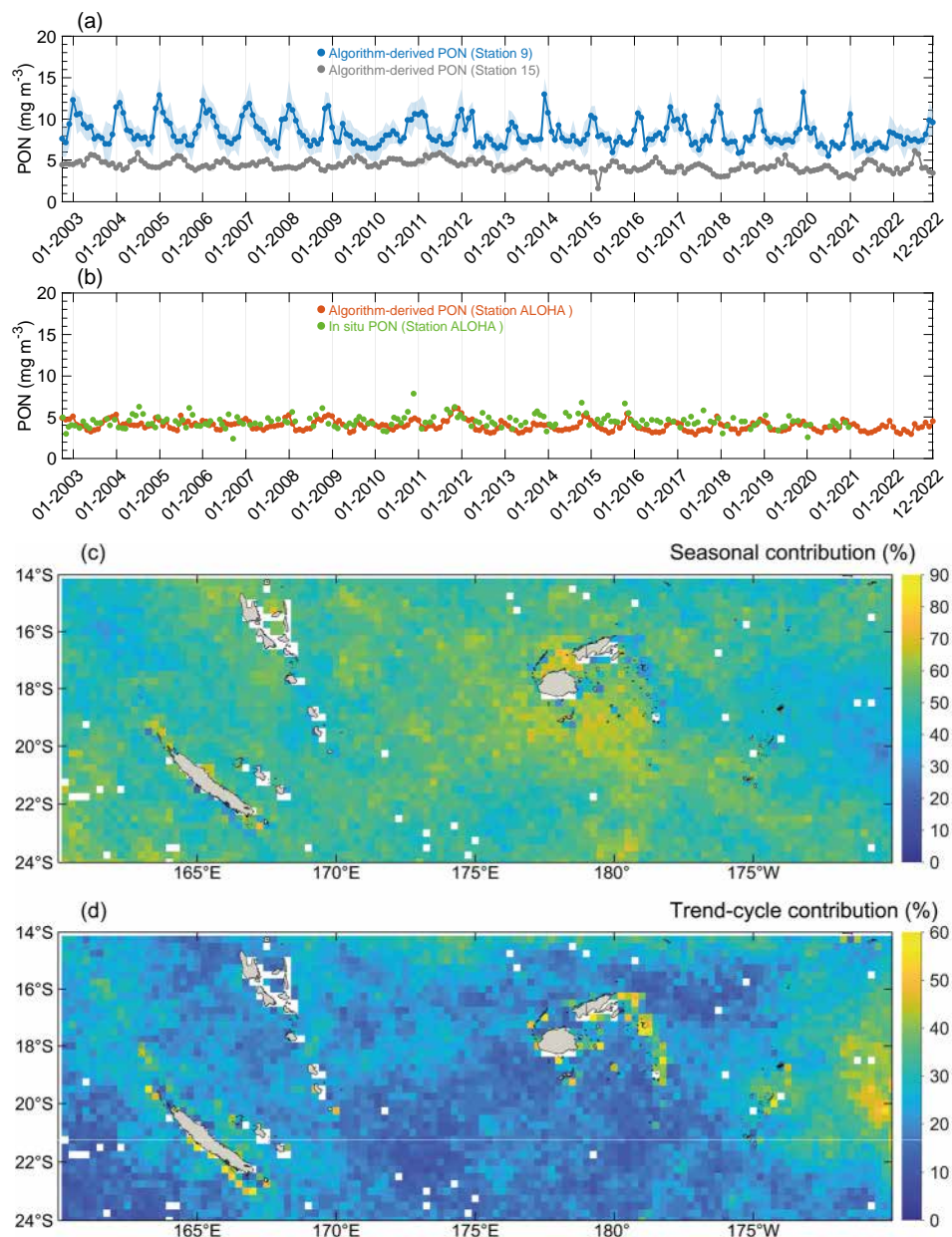
### Comparison between the algorithm-derived and measured PON

Figure 1a shows a map of monthly average algorithm-derived PON concentrations in the South Pacific over the time period of the OUTPACE cruise<sup>9</sup>. For comparison, the field surface PON measurements collected during the cruise and not used in the development of the algorithm are also shown (colored markers). The application of the  $a_{ph}(442)$ -based algorithm to the satellite ocean color observations reveals a global pattern of PON distribution consistent with the expected geographical distribution observed in situ during the OUTPACE cruise. Relatively elevated PON ranging from 8 to 14  $mg\ m^{-3}$  are observed in the western part of the South Pacific bounded between southern New Caledonia at 22°S to northern Vanuatu and Fiji Islands at 14°S and between 160°E and 170°W (black solid box on Fig. 1a). In striking contrast, very low concentrations, 2 to 3 times lower than those in the Melanesian archipelago, are found to the east of the Tonga-Kermadec arc within the South Pacific Gyre (black dashed box on Fig. 1a). The results in Fig. 1a demonstrate the ability of the  $a_{ph}(442)$ -based algorithm to effectively reproduce contrasting spatial patterns of PON concentrations between these two distinct biogeochemical provinces. It is worth noting that at the spatial and temporal scale of the OUTPACE cruise, both algorithm-derived POC and chlorophyll-a concentrations follow the same spatial patterns as PON, with a clear



**Fig. 1 | Surface mass concentrations of particulate organic nitrogen (PON) in the tropical South Pacific in March 2015.** Average 1-month (March 2015) composite images of (a) algorithm-derived PON concentrations ( $mg\ m^{-3}$ ) in surface waters of the tropical South Pacific. The black solid and dashed boxes refer to the Melanesian archipelago and the South Pacific Gyre areas, respectively. The red box corresponds to the region defined as  $N_2$  fixation hotspot<sup>16</sup>. **b** Station-by-station

comparison between the algorithm-derived PON concentrations ( $mg\ m^{-3}$ ) (blue squares) and the surface in situ PON concentrations measured in the mixed layer during the OUTPACE cruise (green circles). Shaded regions show standard deviation around the satellite mean derived PON concentrations. Error bars show standard deviation around the in situ PON concentrations.



**Fig. 2 | Temporal variability of surface mass concentrations of particulate organic nitrogen (PON).** **a** Temporal variations of monthly PON concentrations ( $\text{mg m}^{-3}$ ) in surface waters as indicated with blue and grey colors corresponding to the Melanesian archipelago (station 9 on Fig. 1a), South Pacific Gyre (station 15 on Fig. 1a) datasets, respectively. **b** Temporal variations of monthly PON concentrations in surface waters of the Station ALOHA (black triangle on Extended data

Fig. 4). Shaded regions show standard deviation around the mean. The green circles refer to the surface in situ PON concentrations measured at the Station ALOHA. **c** Contribution of the seasonal, and **(d)** trend components to the total variance of PON in the Melanesian archipelago region (black solid box on Fig. 1a) as calculated with the Census X-II method applied on the monthly time series between December 2002 and December 2022.

distinction between the biomass-rich waters of the Melanesian archipelago and the oligotrophic waters of the gyre (Supplementary Fig. 1 and Fig. 2).

To evaluate the regional performance of the  $a_{\text{ph}}(442)$ -based algorithm, a station-by-station comparison was performed between the algorithm-derived and the measured PON in the western tropical South Pacific (Fig. 1b). We applied the  $a_{\text{ph}}(442)$ -based algorithm to satellite data with an 8-day temporal resolution and a 25 km spatial resolution. The station-by-station comparison reveals excellent agreement between PON derived from algorithms and measured PON over the whole range of longitudinal variability measured during the OUTPACE cruise. Relatively high values are observed in the Melanesian

archipelago, especially at station B, followed by a sharp decrease in values between stations 13 and 15. The best-fit regression functions of algorithm-derived vs. measured PON align closely with the 1:1 line (Supplementary Fig. 3). The aggregate bias is negligibly small with a median ratio,  $\text{MdR} = 0.97$ . For all stations,  $a_{\text{ph}}(442)$  reproduce the PON variability with a median absolute percentage difference,  $\text{MdAPD}$ , values slightly below 15% (Supplementary Table 1). Although PON is associated with both phytoplankton and non-algal organic particles and the  $a_{\text{ph}}(\lambda)$  are intended to represent the light absorption only by phytoplankton pigments, these results confirm that  $a_{\text{ph}}(442)$  has the ability to predict PON in the western tropical South Pacific (Supplementary Table 1). This can be explained by the fact that, non-algal

particles (including detritus, bacteria, zooplankton) are generally correlated with phytoplankton biomass<sup>30</sup>. As a result, phytoplankton absorption is expected to be strongly correlated with the overall PON pool in the western tropical South Pacific Ocean. In addition, in this specific environment characterized by intense biological N<sub>2</sub> fixation, most of the new N is rapidly synthesized into the phytoplanktonic biomass. Even if part of N is released to the labile dissolved organic and inorganic pools, it is rapidly re-assimilated by the N-starved organisms<sup>31,32</sup>. Therefore, the PON variability in this region is mostly related to living organic matter, i.e. phytoplankton cells, and to a lesser extent, detritus<sup>24</sup>.

### Temporal variability of surface PON concentrations

The temporal variations of algorithm-derived PON were extracted at two contrasting stations (Fig. 2a): one located in the Melanesian archipelago to the south of Fiji Island (station 9 on Fig. 1a) and the other situated in the waters of the South Pacific Gyre (station 15 on Fig. 1a) over two decades from December 2002 to December 2022. For comparison, Fig. 2b also includes the temporal variations of both in situ (green color) and algorithm-derived PON (red color) extracted in the North Pacific Subtropical Gyre at the Station ALOHA (black triangle on Supplementary Fig. 4).

In the South Pacific Gyre, very low seasonal variations were observed. Indeed, the algorithm-derived PON remained relatively constant throughout the study period, with an average value of  $4.3 \pm 0.6 \text{ mg m}^{-3}$  (Fig. 2a). The concentrations of PON in the North Pacific Gyre were also extremely low ( $4.1 \pm 0.6 \text{ mg m}^{-3}$ ), with very similar values as those observed in the South Pacific Gyre (Fig. 2b), suggesting a relatively steady phytoplankton biomass and associated particles in both regions. It is notable that the algorithm-derived PON agree reasonably well with in situ PON measurements at Station ALOHA, thus confirming the ability of  $a_{\text{ph}}(442)$  to accurately predict PON in oligotrophic subtropical waters over the past two decades. The results are consistent with expectations regarding the variability of PON in open-ocean environments. For example, remarkably stable and low ( $\sim 3 \text{ mg m}^{-3}$ ) surface concentrations of PON have been reported in the South Pacific Gyre at seasonal temporal scales<sup>24</sup>. Similarly, at Station ALOHA in the North Pacific Subtropical Gyre, the concentrations of PON in surface waters average between  $4.3 \text{ mg m}^{-3}$  in spring and  $4.7 \text{ mg m}^{-3}$  in autumn<sup>33</sup>. In these areas, previously defined as permanently stratified subtropical biomes<sup>34</sup>, the low supply of nutrients year-round combined with a probable iron limitation of nitrogen fixation, constrain biological productivity, which is overall primarily limited by nitrogen availability in the region<sup>15</sup>.

In striking contrast, the temporal variation of PON observed in the Melanesian archipelago shows a clear seasonal cycle over the entire observation period (Fig. 2a). Despite interannual variability, the PON generally increases from November to January-February and decreases from March to July-August. During the austral summer (January-February), the maximum PON varies from about 10 and  $14 \text{ mg m}^{-3}$  in the Melanesian archipelago, which is two to three times higher than in the subtropical North and South Pacific Gyres.

Comparison with existing satellite products shows that PON exhibits temporal patterns broadly consistent with satellite-derived POC<sup>35</sup> and chlorophyll-a<sup>28</sup> (Supplementary Fig. 5). Numerous studies have demonstrated that the carbon-to-chlorophyll-a ratio can vary substantially, particularly in oligotrophic regions<sup>36,37</sup>. In contrast, satellite-derived POC and chlorophyll-a display nearly identical seasonal patterns (Supplementary Fig. 5a), with a very strong correlation ( $R^2 = 0.96$ ,  $N = 243$ ; Supplementary Fig. 6a), reflecting their common derivation from similar remote-sensing reflectance,  $R_{\text{rs}}(\lambda)$ , band-ratio algorithms<sup>38</sup>. Algorithm-derived PON displays only a moderate correlation with chlorophyll-a ( $R^2 = 0.43$ ,  $N = 243$ ; Supplementary Fig. 6b), with noticeable offsets during the austral winter (Supplementary Fig. 5b). Such wintertime increases in chlorophyll-a have already been

reported in the western tropical South Pacific<sup>24</sup>. However, while chlorophyll-a exhibited a pronounced seasonal cycle with higher values during the austral winter, PON concentrations over the same period remained relatively constant and low. This decoupling indicates that winter increases in chlorophyll-a largely reflect physiological responses to light limitation rather than actual biomass accumulation<sup>39,40</sup>, potentially leading to biased estimates of new biomass production<sup>24</sup>. Although our PON product may also be subject to some degree of photoacclimation, the effect appears to be small. For example, in the South Pacific Gyre, where biomass remains relatively constant over time<sup>24</sup>, PON concentrations exhibited only minor winter increases ( $< 1 \text{ mg m}^{-3}$ ; Fig. 2a), which are negligible compared to the much larger variability observed in the Melanesian archipelago. This supports the robustness of the PON algorithm in capturing biologically driven dynamics, such as N<sub>2</sub> fixation, with minimal interference from physiological light responses.

The Census X-II method was applied in the selected region of the Melanesian archipelago spanning from New Caledonia to the Tonga volcanic arc (within the black box on Fig. 1a). In the Melanesian archipelago, the seasonal component accounts for most of the total variance, with an average contribution of  $50 \pm 7\%$  (Fig. 2c). The area where the seasonality in the data is maximal is located in the south of the Fiji Islands, with a variance contribution ranging between 28 and 70 % of the total variance. It is important to emphasize that the observed seasonal production of biomass in the Melanesian archipelago occurs in surface waters despite no winter replenishment of nitrate (NO<sub>3</sub><sup>-</sup>) to surface waters<sup>15</sup>. Observations from the OUTPACE<sup>15</sup>, TONGA<sup>16</sup>, and the GLODAPv2.2<sup>41</sup> (Supplementary Fig. 7) datasets indicate that no NO<sub>3</sub><sup>-</sup> was quantified (limit of quantification =  $0.05 \mu\text{M}$ ) in the top 100 m of the water column in this region. This is because the deepening of the mixed layer depth (MLD) which averages 70 m during the winter mixing period (black and light blue lines on Supplementary Fig. 7), is insufficient to reach the nitracline ( $\sim 100 \text{ m}$ )<sup>15</sup>. However, the deepening of the MLD is sufficient to reach the phosphocline ( $\sim 30 \text{ m}$ )<sup>15</sup>. Consequently, the seasonal winter mixing plays a significant role in providing excess PO<sub>4</sub><sup>3-</sup> relative to NO<sub>3</sub><sup>-</sup> to the upper waters, and therefore in controlling N input by N<sub>2</sub> fixation<sup>15</sup>.

Apart from the role of winter mixing in supplying nutrients, it is important to assess the contribution of potential additional sources of NO<sub>3</sub><sup>-</sup> to surface waters. In this context, we considered the potential role of vertical turbulent diffusion of NO<sub>3</sub><sup>-</sup>. During the OUTPACE cruise, in situ microstructure measurements, including estimates of the vertical diffusion coefficient, were performed within the upper 800 m of the water column<sup>42</sup>. Based on these measurements, theoretical NO<sub>3</sub><sup>-</sup> inputs from deep waters through turbulent diffusion at the top of the nitracline ( $\sim 100 \text{ m}$ ) were estimated<sup>6</sup>. These observations indicated that vertical turbulent diffusion may provide only a minimal contribution (1–8%) to new nitrogen inputs in the photic layer of the western tropical South Pacific, far lower than the contribution from N<sub>2</sub> fixation. Given that the nitracline depth ( $\sim 100 \text{ m}$ ) has remained relatively stable in this region<sup>15</sup> (Supplementary Fig. 7), such low NO<sub>3</sub><sup>-</sup> fluxes are expected to have had no significant impact on biomass production within the upper 0–50 m of the water column, where most N<sub>2</sub> fixation occurs<sup>12,13,16</sup>.

Beyond vertical turbulent diffusion processes, atmospheric deposition may also represent a potential external source of nitrogen to surface waters. It is worth noting that the western tropical South Pacific receives among the lowest levels of atmospheric nitrogen deposition worldwide<sup>43–45</sup>. During the OUTPACE cruise, atmospheric nitrogen deposition fluxes in the Melanesian archipelago ranged between 0.51, and  $0.90 \mu\text{mol N m}^{-2} \text{ d}^{-1}$ , which are  $\sim 3$  orders of magnitude lower than the N<sub>2</sub> fixation rates measured during the same cruise<sup>6</sup>. These results indicate that atmospheric deposition accounted for  $< 1.5\%$  of the total new nitrogen input to surface waters<sup>6</sup>, confirming its negligible role in the nitrogen budget of this region. In order to

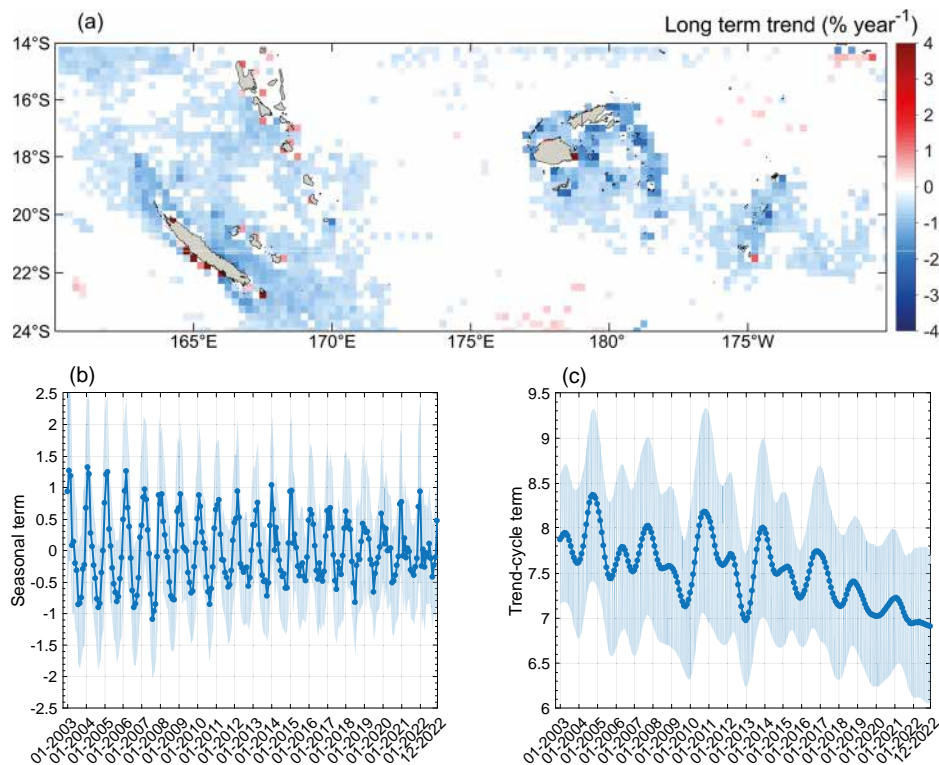


**Fig. 3 | Long term trend of surface mass concentrations of particulate organic nitrogen (PON).** **a** Significant monotonic trend in % per year (seasonal Kendall test,  $p$ -value < 0.05) of surface  $a_{\text{ph}}(442)$  algorithm-derived PON concentrations. **b** Regional averaged Census X-II component of the seasonal term ( $\text{mg m}^{-3}$ ) and **(c)**

of the trend-cycle term ( $\text{mg m}^{-3}$ ). The shaded area around the line represents the inter-pixel variability at a given date, and not the statistical uncertainty of the trend estimate.

account for potential temporal variability in atmospheric deposition over the study period, we analyzed satellite-derived Absorbing Aerosol Index (AAI)<sup>46</sup> data covering the last two decades (see Method). Supplementary Fig. 8 presents the mean AAI over the period 1995–2022. The average AAI values over the Melanesian archipelago and the surrounding waters of the South Pacific gyre are close to zero or even negative, indicating a persistent absence or extremely low presence of aerosols in the region over the last two decades. The mean AAI values are very low (<0.5) and exhibit a similar temporal pattern in both the Melanesian archipelago and the South Pacific gyre (Supplementary Fig. 8c). This confirms that atmospheric deposition levels are comparable in the archipelagic and gyre waters, supporting the assumption that differences in PON are not driven by variations in atmospheric nitrogen input.

Another source of  $\text{NO}_3^-$  could be provided from the few emerged Tonga islands, potentially supplying additional nutrients. A recent study demonstrates that nutrients of terrestrial origin are not sufficient to sustain blooms of large amplitude in the Melanesian archipelago<sup>16</sup>. The mass effects of these islands tend to be very localized around the islands, with a chlorophyll-*a* patch area of 9–13  $\text{km}^{247}$ , which is far less than the total surface area of the Melanesian archipelago. The results of Fig. 2a, c therefore provide important additional insights by confirming that a seasonal new production of biomass in the whole Melanesian archipelago exists over the last 20 years, likely related to recurrent  $\text{N}_2$  fixation events. This new production is made possible by the supply of iron from the Tonga arc<sup>16</sup> combined with a seasonal input of  $\text{PO}_4^{3-}$  in surface waters<sup>15</sup>.

In addition to the substantial contribution of the seasonal component, the analysis of the spatial patterns in the temporal variability using the Census X-II method reveals that the trend-cycle (inter-annual nonlinear modulation) accounts for  $23 \pm 7$  % of the total temporal variability over the two decades (Fig. 2d). As previously mentioned, the

trend-cycle extracted from the X-II procedures does not contain any additional variations related to inter-annual change in seasonality<sup>48</sup>. Consequently, the X-II trend-cycle component is more effective in capturing the long-term evolution of the mean variable under study, making it particularly suitable for modeling climate variations<sup>49</sup>. Overall, the results shown in Fig. 2d support that, although the temporal variability of PON in the Melanesian archipelago is mainly driven by the seasonal component, there are external factors that partially control the long-term temporal variability of PON. Establishing relationships between long-term trends in new production of biomass and climate variability is beyond the scope of this study. However, it can be hypothesized that changes in climate forcing, such as global climate change or natural oscillations, and consequently changes in the environment in which diazotrophic microorganisms develop, may partly explain the notable contribution of the trend-cycle component to the total variance of the time series.

### Long term trends

We now examine the long-term trend in PON within the Melanesian archipelago region (black solid box on Fig. 1a). For this purpose, we first tested for the presence of monotonic upward/downward significant inter-annual trends (expressed in %/year) in the time series of PON by using the non-parametric seasonal Kendall test. Significant decreasing trends (up to 3%/year) are observed south and east of the Fiji Islands, where the data seasonality is maximal, as well as in the western part of the Melanesian archipelago, particularly north and west of New Caledonia (Fig. 3a). The inter-annual changes of PON, extracted where significant trends are observed, confirm the latter observations. Specifically, the average PON values decrease significantly by  $0.05 \text{ mg m}^{-3} \text{ y}^{-1}$  ( $R = -0.85$ ,  $p$ -value < 0.01) over the last two last decades (Supplementary Fig. 9a). A similar pattern is observed for the median values of the PON (Supplementary Fig. 9b). These results

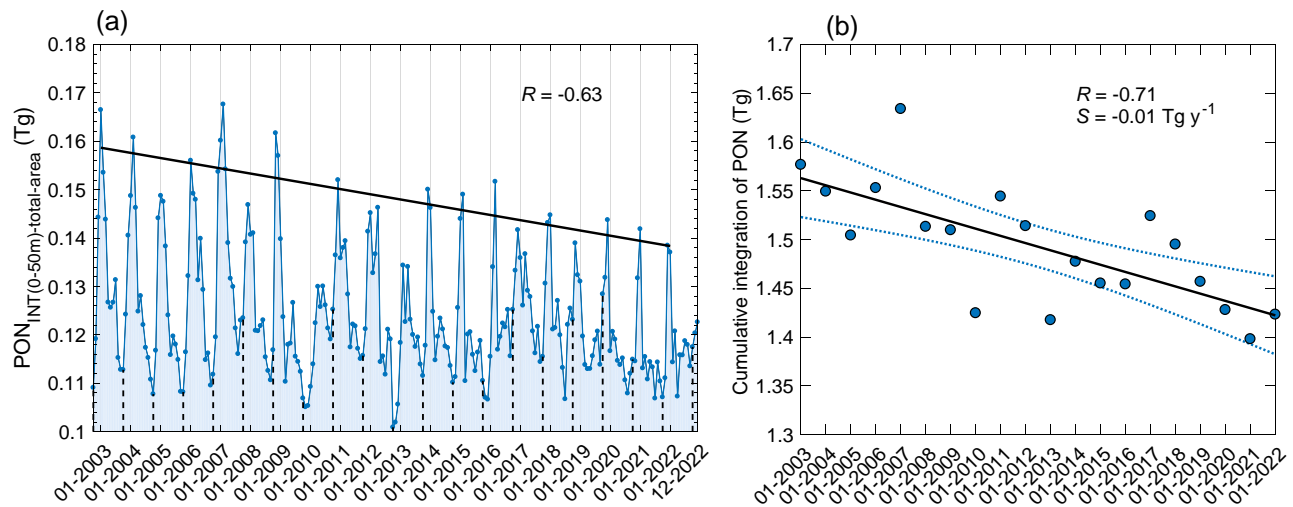


**Fig. 4 | Long term trend of standing stock of particulate organic nitrogen (PON).** **a** Temporal variability of the total area-integrated standing stock of PON ( $\text{PON}_{\text{INT}(0-50\text{m})\text{-total-area}}$ , in unit of Tg). The black solid line is the best-fit function obtained from model-II linear regression between the annual maximum value and time. The panel includes the coefficient of correlation,  $R$ . **b** Cumulative

yearly (from November to October) integration of the  $\text{PON}_{\text{INT}(0-50\text{m})\text{-total-area}}$  within the top 50 m of the study area (red box on Fig. 1a). The black solid line is the best-fit function obtained from model-II linear regression. The panel includes the coefficient of correlation,  $R$ , and the slope,  $S$ , of the best linear fit. Dashed blue lines represent the 95% confidence interval.

indicate a robust decline in PON concentrations in some key areas of the Melanesian archipelago, providing valuable insights on the long-term changes in biomass in this  $\text{N}_2$  fixation hotspot.

The X-II temporal decomposition of the seasonal and trend-cycle terms was applied specifically to the pixels where the seasonal Kendall test identified significant trends ( $p$ -value < 0.05) (Fig. 3b, c). The results of this temporal decomposition show that the significant decreasing trend observed in the Melanesian archipelago (Fig. 3a) is linked to a notable reduction in the amplitude of seasonal fluctuations (Fig. 3b). Specifically, the amplitude of the PON seasonal fluctuations decreases significantly ( $R = -0.87$ ,  $p$ -value < 0.01) between 2003 and 2016, before reaching relatively stable values between 2016 and 2022 (Supplementary Fig. 10). The amplitude of the annual cycle of the seasonal term averaged over 2016-2022 is therefore 55% lower than the averaged one over 2003-2005 (Fig. 3b; Supplementary Fig. 10).

Along with the decrease in seasonal amplitude, the results of the X-II temporal decomposition indicate an associated decline in the trend-cycle term between 2003 and 2022 (Fig. 3c). The trend-cycle term decreases by -10% between 2003 and 2022, indicating a decline in PON in the Melanesian archipelago region.

We then examined the trend of the total area-integrated water column standing stock of PON in the upper 50 m ( $\text{PON}_{\text{INT}(0-50\text{m})\text{-total-area}}$ ) within the region influenced by natural iron supply from the Tonga arc, identified as  $\text{N}_2$  fixation hot spot<sup>16</sup> (red box on Fig. 1a). As expected, similar to surface PON concentrations, the analysis of seasonal variations in  $\text{PON}_{\text{INT}(0-50\text{m})\text{-total-area}}$  (in unit of Tg) shows a recurring seasonal cycle from 1 year to the next, with increases from November to January-February and decrease from March to July-August (Fig. 4a). Despite interannual variability potentially linked to interannual fluctuations in  $\text{PO}_4^{3-}$  and/or iron inputs in surface waters, it is remarkable that the maximum values of peaks observed each year decrease significantly over time ( $R = -0.63$ ,  $p$ -value < 0.01, Fig. 4a).

To evaluate interannual changes in  $\text{PON}_{\text{INT}(0-50\text{m})\text{-total-area}}$ , we calculated an approximation of the cumulative annual integration of  $\text{PON}_{\text{INT}(0-50\text{m})\text{-total-area}}$  using the trapezoidal method with temporal unit spacing (see Method). The  $\text{PON}_{\text{INT}(0-50\text{m})\text{-total-area}}$  values have been integrated over 12 months, for each year and including a complete seasonal cycle (from November to October). The analysis revealed a clear long-term decline in the cumulative annual integration of the

total area-integrated standing stock of  $\text{PON}_{\text{INT}(0-50\text{m})\text{-total-area}}$  (in unit of Tg) within the top 50 m over the two last decades (Fig. 4b). The estimate of the rate of decrease is  $-0.010 \pm 0.002 \text{ Tg y}^{-1}$  ( $p$ -value < 0.01), corresponding to an approximate reduction of 10% in the initial stock within the last 20 years. Overall, this declining trend in  $\text{PON}_{\text{INT}(0-50\text{m})\text{-total-area}}$  (Fig. 4b), coupled with the reduced amplitude of seasonal PON fluctuations (Fig. 3b), provides strong evidence of diminishing seasonal biomass production in the Melanesian archipelago. Given that the surface waters of the western tropical South Pacific are consistently nitrogen-depleted<sup>13,15,50</sup> (Supplementary Fig. 7), these findings suggest a reduction of the input of N via  $\text{N}_2$  fixation over time, potentially driven by changes in the availability of limiting nutrients, and/or in environmental conditions following anthropogenic or natural climate alteration.

### Summary and implications for the biological carbon pump

Using a new bio-optical model based on  $a_{\text{ph}}(442)$  coefficient, estimated from satellite ocean color observations, an optical proxy of PON was derived providing a long-term (December 2002-December 2022) survey of biomass in the subtropical Pacific Ocean. Our results reveal that, over the past two decades, PON concentration was remarkably low in the surface waters of the North and South Pacific Gyres. In these regions, the absence of phytoplanktonic blooms is attributed to  $\text{NO}_3^-$  limitation<sup>15,50</sup>, while  $\text{N}_2$  fixation is likely constrained by limited iron and/or phosphate availability<sup>15,51,52</sup>. In contrast, the temporal analysis of PON concentration within the  $\text{NO}_3^-$ -depleted surface waters of the Melanesian archipelago<sup>15</sup> highlighted a temporally variable new production of biomass over the past 20 years, likely driven by seasonal  $\text{N}_2$  fixation. Previous studies have demonstrated that diazotrophic microorganisms significantly contribute to carbon sequestration in the deep ocean within the Melanesian archipelago<sup>6,53</sup>, with the BCP almost exclusively sustained by  $\text{N}_2$  fixation on a seasonal timescale<sup>15</sup>. Our findings suggest that the seasonal excess of new biomass production in the Melanesian archipelago, compared to the North and South Pacific Gyres, may contribute to the BCP and carbon sequestration over longer time-scale.

Our results reveal that over the last two decades there has been a gradual decline in biomass within this  $\text{N}_2$  fixation hotspot of the Melanesian archipelago. This decline is attributed to a reduction in the

amplitude of seasonal cycles over time, indicating that seasonal nitrogen inputs via  $N_2$  fixation are decreasing and/or the seasonal export of PON are increasing. This trend inevitably leads to a significant reduction of nitrogen available to primary producers and to the entire food web. Such a reduction could contribute to a decline in oceanic carbon sequestration in the future, with potential implications for biogeochemical cycles and climate regulation. Our observations suggest a shift of the BCP out of its equilibrium state which need to be studied on a more global perspective. Our results closely agree with those observed in the northwestern Pacific Ocean<sup>19</sup> where, based on the comparison of sediment trap data with physical and biogeochemical variables, the authors have shown that the magnitude of the springtime BCP has reduced with time due to a corresponding decrease in the biomass of cyanobacterial  $N_2$  fixers<sup>19</sup>.

Although no long-term monitoring of iron inputs to surface waters in the Melanesian archipelago exists over the past two decades, all available measurements consistently indicate elevated iron concentrations in the Melanesian archipelago, regardless of the season considered, compared to the South Pacific gyre<sup>16,51,52</sup>. Recent studies have shown that these relatively high concentrations in the Melanesian archipelago are driven by hydrothermal inputs from the volcanic arc, thereby sustaining iron enrichment<sup>16,54</sup>. In iron-rich surface waters of the Melanesian archipelago, the seasonal variations in the rates of  $N_2$  fixation are ultimately controlled by the concentration of phosphate,  $PO_4^{3-}$  in surface water, which are replenished through seasonal winter mixing<sup>15</sup>. In response to surface ocean warming, increased stratification is expected, which in turn will reduce nutrient fluxes to the upper ocean<sup>55,56</sup>. Based on modeled forecast data from the CMEMS database (E.U. Copernicus Marine Service Information), a decrease in the annual mean depth of the MLD is observed in the Melanesian archipelago, particularly since 2014 (Supplementary Fig. 11). Such an increase in stratification is expected to be accompanied by a decline in the winter supply of  $PO_4^{3-}$  to surface waters. Alongside the increase in stratification, Gerace et al.<sup>56</sup> recently identified a deepening of the pycnocline, especially throughout the southern hemisphere, leading to increasing phosphorus stress for marine phytoplankton. Consequently, although this hypothesis has yet to be confirmed, a reduction in seasonal  $PO_4^{3-}$  inputs through winter mixing appears to be the most plausible explanation for the observed decrease in annual biomass production in the Melanesian archipelago.

In closing, as pointed out in previous studies<sup>17,57–59</sup>, our results indicate that the productivity of the ocean, and hence the strength of the BCP, may be deviating from its previous equilibrium condition. Nevertheless, it is important to stress that the magnitude and direction of future changes in the  $N_2$  fixation process and the BCP remains uncertain. In the broader context, the entire region under study is characterized by warm and persistently stratified surface waters, even during winter, which strongly limit vertical  $NO_3^-$  supply but simultaneously favor diazotrophs. Such conditions are expected to become more frequent in warmer and increasingly stratified nutrient-poor surface waters projected for the future, which could in turn favor diazotrophs and potentially enhance overall productivity<sup>18,55,60</sup>. Our study demonstrates that the use of ocean satellite color data offers a promising alternative to discrete measurements for assessing trends in biomass in regions influenced by  $N_2$  fixation, especially in response to surface ocean warming. Climate-induced changes in the ocean have the potential to affect  $N_2$  fixation hotspots across the global ocean. A next step for this research would be to evaluate long-term trend in biomass using ocean color data in various hotspots of  $N_2$  fixation across the global ocean. Such analyses could improve our understanding and predictive capability regarding the responses of  $N_2$  fixation and the BCP to global climate change.

## Methods

### In situ measurements

A dataset of in situ measurements of mass concentrations of surface (<10 m) particulate organic nitrogen (PON) was compiled from multiple open access databases covering the period from 1997 to 2023 (Supplementary Table 2). Nearly all PON measurements are here considered as the particulate nitrogen retained by a pre-combusted Whatman GF/F filter according to the JGOFS (Joint Global Ocean Flux Study) protocol<sup>61</sup>. The exceptions were the “Oligotrophy to Ultra-oligotrophy PACific Experiment”, OUTPACE<sup>9</sup>, and the “shallow hydro-Thermal sources of trace elements-potential impacts on the biological productivity and biological carbon pump”, TONGA<sup>62</sup>, datasets, where PON measurements were quantified spectrophotometrically using the wet oxidation method based on persulfate digestion at 120 °C<sup>63</sup>. PON concentrations obtained using the wet oxidation method has been shown to yield results consistent with the standard JGOFS/CHN protocol<sup>64,65</sup>, ensuring methodological consistency for algorithm validation. To further evaluate this, we analyzed six oligotrophic seawater samples using both the wet oxidation and CHN methods applied during the OUTPACE cruise (Supplementary Table 3). Importantly, the results confirmed that PON concentrations obtained by the wet oxidation method are consistent with those from CHN analysis, within the expected uncertainty for oligotrophic waters.

In situ nitrate and phosphate measurements were extracted from the open-access Global Ocean Data Analysis Project version 2.2 (GLODAPv2.2) dataset<sup>41</sup>. These data correspond to the Melanesian Archipelago region, spanning latitudes 14°S to 24°S and longitudes 160°E to 170°W.

### Ocean color data and PON algorithms

We used the GlobColour daily merged L3 Ocean Color remote sensing reflectance,  $R_{rs}(\lambda)$ , (in  $sr^{-1}$ , where  $\lambda$  is light wavelength in vacuum) at 4 km × 4 km of spatial resolution<sup>28</sup> ([https://hermes.acri.fr/images/GlobCOLOUR\\_PUG.pdf](https://hermes.acri.fr/images/GlobCOLOUR_PUG.pdf)) collected from 1997 to 2023. We also used the GlobColour daily merged L3 chlorophyll-a concentrations at the same spatial resolution and time period<sup>28</sup>. Particulate organic carbon (POC) concentrations were estimated from  $R_{rs}(\lambda)$  using the algorithm developed by Stramski et al.<sup>35</sup>. Empirical PON algorithm was developed by using the spectral absorption coefficients of phytoplankton,  $a_{ph}(442)$  estimated from  $R_{rs}(\lambda)$  using a three-step inverse model (3SAA)<sup>26,27</sup>. The satellite  $a_{ph}(442)$  were extracted over in situ PON measurements to generate the match-up dataset (Supplementary Fig. 12a). This dataset was computed following the Eumetsat validation protocols (EUM/SEN3/DOC/19/1092968)<sup>66</sup> which is in agreement with the NASA Ocean Color protocol<sup>67</sup>. The matchups between satellite  $a_{ph}(442)$  and PON in situ measurements were performed within a 3 × 3 pixel-box centered at the location of the field station, and a minimum of 5 valid pixels with a coefficient of variation <0.15 were required to keep the match-up data point. This final dataset of 1979 matchup data points was divided into two parts: 70% for the model development dataset, (N = 1376, red markers on Supplementary Fig. 12a), and 30% for the model validation (N = 603, blue markers on Supplementary Fig. 12a). It should be noted that the frequency distribution of PON and  $a_{ph}(442)$  is comparable for the model and validation datasets (Fig. not shown).

In this study, model-II linear regression using the major axis method<sup>68,69</sup> was applied to the  $\log_{10}$ -transformed PON and  $a_{ph}(442)$  coefficients derived from satellite data, to determine predictive relationships for PON (in unit of  $mg\ m^{-3}$ ) as a function of  $a_{ph}(442)$ . From these analyses, we present the best-fit equations in the form of a power function. The general formula of the power function is:

$$PON = 226.58 a_{ph}(442)^{0.78} \quad (1)$$

The goodness-of-fit of regression equation was evaluated through the analysis of algorithm-derived PON vs. measured PON using independent satellite sensor-specific validation dataset. For this evaluation, model-II linear regression analysis was performed using the major axis method<sup>68,69</sup> applied to the data of algorithm-derived vs. measured PON. Additionally, this evaluation involves calculating several statistical metrics that quantify the differences between algorithm-derived and measured values of PON (Supplementary Table 4). Supplementary Fig. 12b supports a reasonably good agreement between PON derived from  $a_{ph}(442)$  and measured PON over the whole range of variability observed within the whole dataset. Deviation between the linear fit of the relationships between the  $a_{ph}(442)$ -algorithms derived PON and measured PON and the 1:1 line is very low (Supplementary Fig. 12b). The slopes,  $S$ , reach very high values ( $S = 0.94$ ) and the coefficient of correlation,  $R$ , also shows high values ( $R = 0.88$ ). The MdAPD and MdSA, values of the  $a_{ph}(442)$ -algorithm PON vs. measured PON relationships are 26.15 % and 30.10 %, respectively. Overall, this indicates that  $a_{ph}(442)$  has the potential to be used as predictive variable in  $a_{ph}(442)$ -based algorithms for estimating PON over a wide range of oceanic environments.

### Absorbing Aerosol Index (AAI)

The Absorbing Aerosol Index (AAI) dataset provide from the Multi-Sensor Absorbing Aerosol Index (MS-AAI) data record ([https://www.temis.nl/airpollution/absaai/#GOME2\\_AAI](https://www.temis.nl/airpollution/absaai/#GOME2_AAI)), which consists of AAI data from the TOMS, GOME-1, SCIAMACHY, OMI, GOME-2A, GOME-2B, and GOME-2C instruments. The AAI is based on the difference in reflectance measurements at two wavelengths, typically around 340 nm and 380 nm<sup>46</sup>. The aerosol types that are mostly seen in the AAI are desert dust and biomass burning aerosols. By comparing the measured UV reflectance with the theoretical reflectance expected in a purely Rayleigh-scattering atmosphere (i.e., without absorbing aerosols), the AAI provides a qualitative estimate of the presence and intensity of UV-absorbing aerosols. When a positive residue is found, absorbing aerosols were detected. Negative or zero residues on the other hand suggest an absence of absorbing aerosols.

### Mixed layer depth (MLD)

The MLD values were extracted at each station from the Multi-Observation Global Ocean ARMOR3D L4 reanalysis product (<https://doi.org/10.48670/moi-00052>)<sup>70,71</sup> which provides temperature and salinity profiles interpolated onto a regular grid, and is suitable for large-scale, long-term analyses. As the ARMOR3D L4 MLD product does not cover the earliest field cruises, we complemented our dataset with MLD values derived from the global climatology developed by<sup>72</sup>. It should be noted that both MLD values were calculated using a threshold criterion of a 0.2 °C temperature deviation from the reference value at 10 m depth.

### Time series analysis

In the present study, the monthly time series of PON have been temporally decomposed using the Census X-11 method. This method has been introduced for the analysis of sea surface temperature<sup>49</sup> and has been extensively documented for various ocean color applications<sup>29,48,73–76</sup>. This approach is of interest for precisely describing the temporal variation patterns in a time series. The iterative analysis based on the successive application of bandpass filters aims at decomposing the time series into three additive components representing the seasonal, the trend-cycle (inter-annual modulation), and irregular (or residual) modulations in the data. The relative part of the variance of the components is estimated for each grid point, to identify the spatial patterns of the temporal variability in the series.

In addition, we tested for the presence of monotonic upward or downward significant inter-annual trends in the time series of PON. We used the non-parametric seasonal Kendall test, based on the

calculation of a set of Mann-Kendall statistics applied to each separate month, which are then combined to evaluate the existence of long-term monotonic changes in the original time series<sup>77</sup>. We used Sen's slope, a non-parametric slope estimator<sup>77,78</sup> to estimate the magnitude of each time series trend, expressed in % per year<sup>79</sup>.

### Estimation of the PON content integrated over the 0–50 m depth layer

Satellite observations of ocean color provide information restricted to the first optical depth. However, diazotrophic activity occurs not only in surface waters but also throughout the upper water column. In the western tropical South Pacific,  $N_2$  fixation have been consistently detected in the top 50 m of the photic layer<sup>12–14</sup>. To estimate and evaluate the long-term trend of standing stock of PON in the upper 50 m water column from satellite observations, it is possible to develop an empirical relationship to derive PON content integrated over the 0–50 m depth layer, and then apply it to satellite observations of ocean color. Similar empirical relationship between near-surface POC concentrations and POC content integrated over the euphotic zone have been developed to assess the integrated content of POC over the global ocean from satellite observations<sup>35</sup>. In the Southern Ocean, the area-integrated water column standing stock of POC have been estimated in the upper 100 m water column from empirical relationship between surface POC concentrations and POC integrated within the 0–100 m depth layer<sup>80</sup>.

In the present study, we develop an empirical relationship between in situ near-surface PON concentrations and the PON content integrated over the 0–50 m depth layer by using the OUTPACE and TONGA datasets. The OUTPACE cruise was conducted during the austral summer, from February 18 to April 3, 2015, along a 4000 km zonal transect from north of New Caledonia to the western part of the South Pacific Gyre<sup>9</sup>. Along this transect, 18 stations were sampled (black circle on Supplementary Fig. 4). The TONGA dataset includes PON measurements collected in the western tropical South Pacific in November 2019 along a west-to-east transect<sup>61</sup> (white square on Supplementary Fig. 4). We assume that the 50 m depth boundaries the biologically active layer where the majority of PON production sustained by  $N_2$  fixation takes place in the Melanesian archipelago. Our field data show that the surface PON concentration is reasonably well correlated with the PON integrated within the 0–50 m depth layer (Supplementary Fig. 13). The coefficient of determination between the  $\log_{10}$ -transformed data is high ( $R^2 = 0.91$ ) and the pattern of data suggests that the relationships can be well described by a power function (blue line Supplementary Fig. 13):

$$PON_{INT(0-50m)} = 63.62 \times PON^{0.80} \quad (2)$$

For comparison, Supplementary Fig. 13 includes the relationship established in the North Pacific subtropical gyre using in situ measurements of PON performed over two decades from December 2002 to December 2022 as part of the Hawaii Ocean Time-series, HOT, program at Station ALOHA (black triangle on Supplementary Fig. 4). It is notable that the best-fit power functions for the  $PON_{INT(0-50m)}$  vs. PON are similar for the whole dataset and its subsets, HOT and OUTPACE/TONGA datasets. This indicates, on one hand, that the  $PON_{INT(0-50m)}$  vs. PON relationship is consistent for different subtropical regions of the open ocean, and on the other hand, that it shows relatively low variability over time.

Therefore, based on these observations, the relationship established in the western tropical South Pacific has been applied to satellite-derived monthly surface PON concentration in order to estimate the integrated water column standing stock of PON within the upper 50 m. Details of the method used to estimate the total area-integrated standing stock of PON within the top 50 m of the column waters of the study area are provided below. The first step involves

estimating the integrated water column standing stock of PON within the upper 50 m ( $\text{PON}_{\text{INT}(0-50\text{m})}$ , in unit of  $\text{mg m}^{-2}$ ) for each pixels in a restricted area of the western tropical South Pacific (red box on Fig. 1a). This corresponds to the area recently defined as  $\text{N}_2$  fixation hotspot<sup>16</sup>. According to these authors, the fluids emitted from the Tonga volcanic arc have a substantial impact on iron concentrations in the photic layer. The natural iron fertilization fuels regional hotspot of  $\text{N}_2$  fixation which extend 800 km in longitude and 400 km in latitude ( $\sim 360\,000\text{ km}^2$ ). The region defined as the hotspot of  $\text{N}_2$  fixation was divided into sections of  $1.5^\circ$  of longitude and  $1^\circ$  of latitude, which is reasonably limited in terms of spatial extent. As a result, each satellite derived monthly maps of mass of  $\text{PON}_{\text{INT}(0-50\text{m})}$  was divided into 16 sectors of 35 pixels each. As satellite data are not available at any given time, the number of valid pixels varies from one sector to another. It should be noted that each sector contains a sufficient number of valid pixels to calculate an average value of monthly mean of  $\text{PON}_{\text{INT}(0-50\text{m})}$  in each sectors ( $\text{PON}_{\text{INT}(0-50\text{m})\text{-sector}}$ , in unit of  $\text{g m}^{-2}$ ).

$$\text{PON}_{\text{INT}(0-50\text{m})\text{-sector}} = \frac{1}{N_p} \sum \text{PON}_{\text{INT}(0-50\text{m})} \quad (3)$$

Given the relatively small surface area of each sector, we assume that the data from the valid pixels provide an average value of  $\text{PON}_{\text{INT}(0-50\text{m})}$ .  $N_p$  is the number of valid pixels in each section. The next step was to calculate the area-integrated value of water column PON within each sector ( $\text{PON}_{\text{INT}(0-50\text{m})\text{-sector-area}}$ , in unit of g). For that purpose, the  $\text{PON}_{\text{INT}(0-50\text{m})\text{-sector}}$  has been multiplied by the surface area ( $S$ , in unit of  $\text{m}^2$ ) of each sector.

$$\text{PON}_{\text{INT}(0-50\text{m})\text{-sector-area}} = \text{PON}_{\text{INT}(0-50\text{m})\text{-sector}} \times S \quad (4)$$

The final step involves calculating the total area-integrated standing stock of PON within the top 50 m of the column waters of the study area,  $\text{PON}_{\text{INT}(0-50\text{m})\text{-total-area}}$  (in unit of g). Afterwards,  $\text{PON}_{\text{INT}(0-50\text{m})\text{-total-area}}$  was converted to Tg ( $1\text{ Tg} = 10^{12}\text{ g}$ ).

$$\text{PON}_{\text{INT}(0-50\text{m})\text{-total-area}} = \sum \text{PON}_{\text{INT}(0-50\text{m})\text{-sector-area}} \quad (5)$$

## Data availability

The Ocean Color satellite data used in this study are publicly available from the online GlobColour repositories: <https://hermes.acri.fr/index.php?class=archive>. The in situ measurements of surface mass concentrations of particulate organic nitrogen (PON) used in this study are publicly available from the following data repositories: the Biological and Chemical Oceanography Data Management Office (<https://www.bco-dmo.org/>), the Global Ocean Particulate Organic Phosphorus, Carbon, Oxygen for Respiration, and Nitrogen (<https://doi.org/10.5061/dryad.d702p>, <https://doi.org/10.5061/dryad.05qftf5h>), the LEFE-CYBER database (<https://www.obs-vlfr.fr/proof/cruises.php>; OUTPACE and TONGA cruises), the NASA SeaWiFS Bio-optical Archive and Storage System (<https://seabass.gsfc.nasa.gov/>; HLY1001, HLY1101), the PANGAEA Data Publisher for Earth and Environmental Science (<https://doi.org/10.1594/PANGAEA.902230>; ANTXXVI/4, KMI2-10), the Data and Sample Research System for Whole Cruise Information database of the Japan Agency for Marine-Earth Sciences (<https://doi.org/10.17596/0001879>; MR1705-C), the SEA scieNtific Open data Edition (<https://www.seaodc.org/data/00824/93570/>; COASTIOOC), the Bermuda Atlantic Time-series Study (<https://bats.bios.edu/>), the Hawaii Ocean Time-series (<https://hahana.soest.hawaii.edu/hot/>), and the French coastal monitoring SOMLIT network (<https://www.somlit.fr/>). The Absorbing Aerosol Index (AAI) dataset is publicly available from the open access online data repositories ([https://www.temis.nl/airpollution/absaaai/#GOME2\\_AAI](https://www.temis.nl/airpollution/absaaai/#GOME2_AAI)). Temperature and salinity data

used to calculate the mixed layer depth are publicly available from the Multi-Observation Global Ocean ARMOR3D Level 4 reanalysis product (<https://doi.org/10.48670/moi-00052>). The raw data underlying all main figures have been deposited in the public repository (<https://doi.org/10.5281/zenodo.17541762>). The code used to estimate seawater inherent optical properties, including the spectral absorption  $a(\lambda)$  and backscattering  $b_b(\lambda)$  coefficients and their non-water components  $a_{\text{nw}}(\lambda)$  and  $b_{\text{bp}}(\lambda)$  from remote-sensing reflectance  $R_{\text{rs}}(\lambda)$ , is publicly available online ([https://github.com/SIO-Ocean-Optics-Research-Laboratory/LS2\\_Distribution](https://github.com/SIO-Ocean-Optics-Research-Laboratory/LS2_Distribution)). The code used to derive  $a_{\text{ph}}(\lambda)$  from  $a_{\text{nw}}(\lambda)$  is publicly available online (<https://github.com/TELHYD-LOG/3SAA>). The codes used to decompose the monthly time series of PON (Census X11 method) have been deposited in the public repository (<https://github.com/AlFume13/Census-X11-algorithm/tree/main>). The data and code that support the findings of this study are available from the corresponding author upon request.

## References

- Falkowski, P. G., Barber, R. T. & Smetacek, V. Biogeochemical controls and feedbacks on ocean primary production. *Science* **281**, 200–206 (1998).
- Tyrell, T. The relative influences of nitrogen and phosphorus on oceanic primary production. *Nature* **400**, 525–531 (1999).
- Moore, C. M. et al. Processes and patterns of oceanic nutrient limitation. *Nat. Geosci.* **6**, 701–710 (2013).
- Koeve, W. & Kähler, P. Balancing ocean nitrogen. *Nat. Geosci.* **3**, 383–384 (2010).
- Capone, D. G. et al. Nitrogen fixation by *Trichodesmium* spp.: An important source of new nitrogen to the tropical and subtropical North Atlantic Ocean. *Glob. Biogeochem. Cycles* **19**, GB2024 (2005).
- Caffin, M. et al.  $\text{N}_2$  fixation as a dominant new N source in the western tropical South Pacific Ocean (OUTPACE cruise). *Biogeosciences* **15**, 2565–2585 (2018).
- Karl, D. M. et al. Dinitrogen fixation in the world's oceans. *Biogeochemistry* **57**, 47–98 (2002).
- Forrer, H. J. et al. Quantifying  $\text{N}_2$  fixation and its contribution to export production near the Tonga-Kermadec Arc using nitrogen isotope budgets. *Front. Mar. Sci.* **10**, 1249115 (2023).
- Moutin, T., Doglioli, A. M., De Verneil, A. & Bonnet, S. Preface: The oligotrophy to the ULtra-oligotrophy PACific experiment (OUTPACE cruise, 18 February to 3 April 2015). *Biogeosciences* **14**, 3207–3220 (2017).
- Dupouy, C. et al. Satellite captures *Trichodesmium* blooms in the southwestern tropical Pacific. *EOS, Trans. Am. Geophys. Union* **81**, 13–16 (2000).
- Dupouy, C., Benielli-Gary, D., Neveux, J., Dandonneau, Y. & Westberry, T. K. An algorithm for detecting *Trichodesmium* surface blooms in the South Western Tropical Pacific. *Biogeosciences* **8**, 3631–3647 (2011).
- Bonnet, S. et al. Contrasted geographical distribution of  $\text{N}_2$  fixation rates and *nifH* phylotypes in the Coral and Solomon Seas (south-western Pacific) during austral winter conditions. *Glob. Biogeochem. Cycles* **29**, 1874–1892 (2015).
- Bonnet, S. et al. In-depth characterization of diazotroph activity across the western tropical South Pacific hotspot of  $\text{N}_2$  fixation (OUTPACE cruise). *Biogeosciences* **15**, 4215–4232 (2018).
- Bonnet, S., Caffin, M., Berthelot, H. & Moutin, T. Hot spot of  $\text{N}_2$  fixation in the western tropical South Pacific pleads for a spatial decoupling between  $\text{N}_2$  fixation and denitrification. *Proc. Natl. Acad. Sci. USA* **114**, E2800–E2801 (2017).
- Moutin, T. et al. Nutrient availability and the ultimate control of the biological carbon pump in the western tropical South Pacific Ocean. *Biogeosciences* **15**, 2961–2989 (2018).

16. Bonnet, S. et al. Natural iron fertilization by shallow hydrothermal sources fuels diazotroph blooms in the ocean. *Science* **380**, 812–817 (2023).
17. Iversen, M. H. Carbon export in the ocean: a biologist’s perspective. *Annu. Rev. Mar. Sci.* **15**, 357–381 (2023).
18. Karl, D. M. et al. The role of nitrogen fixation in biogeochemical cycling in the subtropical North Pacific Ocean. *Nature* **388**, 533–538 (1997).
19. Kim, D. et al. The reduction in the biomass of cyanobacterial N<sub>2</sub> fixer and the biological pump in the Northwestern Pacific Ocean. *Sci. Rep.* **7**, 41810 (2017).
20. Stramski, D., Reynolds, R. A., Kahru, M. & Mitchell, B. G. Estimation of particulate organic carbon in the ocean from satellite remote sensing. *Science* **285**, 239–242 (1999).
21. Loisel, H., Nicolas, J. M., Deschamps, P. Y. & Frouin, R. Seasonal and inter-annual variability of particulate organic matter in the global ocean. *Geophys. Res. Lett.* **29**, 49–1-49-4 (2002).
22. Stramska, M. Particulate organic carbon in the global ocean derived from SeaWiFS ocean color. *Deep Sea Res. Part I Oceanogr. Res. Pap.* **56**, 1459–1470 (2009).
23. Hu, C., Lee, Z. & Franz, B. Chlorophyll a algorithms for oligotrophic oceans: a novel approach based on three-band reflectance difference. *J. Geophys. Res. Oceans* **117**, C01011 (2012).
24. Fumenia, A. et al. Optical proxy for particulate organic nitrogen from BGC-Argo floats. *Opt. Express* **28**, 21391–21406 (2020).
25. Fumenia, A., Loisel, H., Reynolds, R. A. & Stramski, D. Relationships between the concentration of particulate organic nitrogen and the inherent optical properties of seawater in oceanic surface waters. *Biogeosciences* **22**, 2461–2484 (2025).
26. Loisel, H. et al. An inverse model for estimating the optical absorption and backscattering coefficients of seawater from remote-sensing reflectance over a broad range of oceanic and coastal marine environments. *J. Geophys. Res. Oceans* **123**, 2141–2171 (2018).
27. Jorge, D. S. et al. A three-step semi analytical algorithm (3SAA) for estimating inherent optical properties over oceanic, coastal, and inland waters from remote sensing reflectance. *Remote Sens. Environ.* **263**, 112537 (2021).
28. GlobColour. *GlobColour User Guide*. [https://hermes.acri.fr/images/GlobCOLOUR\\_PUG.pdf](https://hermes.acri.fr/images/GlobCOLOUR_PUG.pdf). <https://hermes.acri.fr/> (2020).
29. Vantrepotte, V., Loisel, H., Mélin, F., Desailly, D. & Duforêt-Gaurier, L. Global particulate matter pool temporal variability over the SeaWiFS period (1997–2007). *Geophys. Res. Lett.* **38**, L02605 (2011).
30. Karl, D. M. & Björkman, K. M. Dynamics of dissolved organic phosphorus. In *Biogeochemistry Of Marine Dissolved Organic Matter* (eds. Hansell, D. A. & Carlson, C. A.) (Academic Press, 2015).
31. Berthelot, H. et al. Dinitrogen fixation and dissolved organic nitrogen fueled primary production and particulate export during the VAHINE mesocosm experiment (New Caledonia lagoon). *Biogeosciences* **12**, 4099–4112 (2015).
32. Caffin, M., Berthelot, H., Cornet-Barthaux, V., Barani, A. & Bonnet, S. Transfer of diazotroph-derived nitrogen to the planktonic food web across gradients of N<sub>2</sub> fixation activity and diversity in the western tropical South Pacific Ocean. *Biogeosciences* **15**, 3795–3810 (2018).
33. Hebel, D. V. & Karl, D. M. Seasonal, interannual and decadal variations in particulate matter concentrations and composition in the subtropical North Pacific Ocean. *Deep-Sea Res. II* **48**, 1669–1695 (2001).
34. Sarmiento, J. L. et al. Response of ocean ecosystems to climate warming. *Glob. Biogeochem. Cycles* **18**, GB3003 (2004).
35. Stramski, D. et al. Relationships between the surface concentration of particulate organic carbon and optical properties in the eastern South Pacific and eastern Atlantic Oceans. *Biogeosciences* **5**, 171–201 (2008).
36. Loisel, H., Bosc, E., Stramski, D., Oubelkheir, K. & Deschamps, P. Y. Seasonal variability of the backscattering coefficient in the Mediterranean Sea based on satellite SeaWiFS imagery. *Geophys. Res. Lett.* **28**, 4203–4206 (2001).
37. Behrenfeld, M. J., Boss, E., Siegel, D. A. & Shea, D. M. Carbon-based ocean productivity and phytoplankton physiology from space. *Glob. Biogeochem. Cycles* **19**, GB1006 (2005).
38. Duforêt-Gaurier, L., Loisel, H., Dessailly, D., Nordkvist, K. & Alvain, S. Estimates of particulate organic carbon over the euphotic depth from in situ measurements. Application to satellite data over the global ocean. *Deep-Sea Res. Part I: Oceanogr. Res. Pap.* **57**, 351–367 (2010).
39. Letelier, R. M. et al. Temporal variability of phytoplankton community structure based on pigment analysis. *Limnol. Oceanogr.* **38**, 1420–1437 (1993).
40. Winn, C. D. et al. Seasonal variability in the phytoplankton community of the North Pacific Subtropical Gyre. *Glob. Biogeochem. Cycles* **9**, 605–620 (1995).
41. Olsen, A. et al. An updated version of the global interior ocean biogeochemical data product, GLODAPv2.2020. *Earth Syst. Sci. Data* **12**, 3653–3678 (2020).
42. Bouruet-Aubertot, P. et al. Longitudinal contrast in turbulence along a ~19° S section in the Pacific and its consequences for biogeochemical fluxes. *Biogeosciences* **15**, 7485–7504 (2018).
43. Duce, R. A. et al. Impacts of atmospheric anthropogenic nitrogen on the open Ocean. *Science* **320**, 893–897 (2008).
44. Okin, G. S. et al. Impacts of atmospheric nutrient deposition on marine productivity: Roles of nitrogen, phosphorus, and iron. *Glob. Biogeochem. Cycles* **25**, GB2022 (2011).
45. Liu, S. et al. Atmospheric reactive nitrogen deposition to the global ocean during the 2010s: Interannual variation and source attribution. *J. Geophys. Res. Atmos.* **130**, e2024JD042789 (2025).
46. Tilstra, L. G., de Graaf, M., Tuinder, O. N. E., van der A. & Stammes, P. R. J. *Monitoring Aerosol Presence Over A 15 Year Period Using The Absorbing Aerosol Index Measured By GOME-1 Sciamachy, and GOME-2*. [https://d37onar3vnbj2y.cloudfront.net/static/airpollution/absaa/doc/ESA-SP-722\\_Tilstra\\_et\\_al.pdf](https://d37onar3vnbj2y.cloudfront.net/static/airpollution/absaa/doc/ESA-SP-722_Tilstra_et_al.pdf) (2014).
47. Messié, M., Petrenko, A., Doglioli, A. M., Martinez, E. & Alvain, S. Basin-scale biogeochemical and ecological impacts of islands in the tropical Pacific Ocean. *Nat. Geosci.* **15**, 469–474 (2022).
48. Vantrepotte, V. & Mélin, F. Inter-annual variations in the SeaWiFS global chlorophyll a concentration (1997–2007). *Deep-Sea. Res. Part I Oceanogr. Res. Pap.* **58**, 429–441 (2011).
49. Pezzulli, S., Stephenson, D. B. & Hannach, A. The variability of seasonality. *J. Clim.* **53**, 71–88 (2005).
50. Raimbault, P. & Garcia, N. Evidence for efficient regenerated production and dinitrogen fixation in nitrogen-deficient waters of the South Pacific Ocean: impact on new and export production estimates. *Biogeosciences* **5**, 323–338 (2008).
51. Blain, S., Bonnet, S. & Guieu, C. Dissolved iron distribution in the tropical and sub tropical South Eastern Pacific. *Biogeosciences* **5**, 269–280 (2008).
52. Moutin, T. et al. Phosphate availability and the ultimate control of new nitrogen input by nitrogen fixation in the tropical Pacific Ocean. *Biogeosciences* **5**, 95–109 (2008).
53. Bonnet, S. et al. Diazotrophs are overlooked contributors to carbon and nitrogen export to the deep ocean. *ISME J.* **17**, 47–58 (2023).
54. Guieu, C. et al. Iron from a submarine source impacts the productive layer of the Western Tropical South Pacific (WTSP). *Sci. Rep.* **8**, 9075 (2018).
55. Doney, S. C. Plankton in a warmer world. *Nature* **444**, 695–696 (2006).
56. Gerace, S. D., Yu, J., Moore, J. K. & Martiny, A. C. Observed declines in upper ocean phosphate availability. *Proc. Natl. Acad. Sci. USA.* **122**, e2411835122 (2025).

57. Sarmiento, J. L. & Gruber, N. *Ocean Biogeochemical Dynamics* (Princeton University Press, Princeton, 2006).
58. Boyd, P. W. Toward quantifying the response of the oceans' biological pump to climate change. *Front. Mar. Sci.* **2**, 77 (2015).
59. Henson, S. A. et al. Uncertain response of ocean biological carbon export in a changing world. *Nat. Geosci.* **15**, 248–254 (2022).
60. Boyd, P. W. & Doney, S. C. Modelling regional responses by marine pelagic ecosystems to global climate change. *Geophys. Res. Lett.* **29**, 53–153-4 (2002).
61. Knap, A. H., Michaels, A., Close, A. R., Ducklow, H. & Dickson, A. G. *Protocols For The Joint Global Ocean Flux Studies (JGOFS) Core measurements* Vol. 170 (Reprint of Intergovernmental Oceanographic Commission Manuals and Guides, UNESCO, Paris, 1994, 1996).
62. Guieu C. et al. Biogeochemical dataset collected during the TONGA cruise. <https://doi.org/10.17882/88169> (2023).
63. Pujo-Pay, M. & Raimbault, P. Improvement of the wet-oxidation procedure for simultaneous determination of particulate organic nitrogen and phosphorus collected on filters. *Mar. Ecol. Prog. Ser.* **105**, 203–203 (1994).
64. Raimbault, P. & Slawyk, G. A semiautomatic, wet-oxidation method for the determination of particulate organic nitrogen collected on filters. *Limnol. Oceanogr.* **36**, 405–408 (1991).
65. Raimbault, P., Diaz, F., Pouvesle, W. & Boudjellal, B. Simultaneous determination of particulate organic carbon, nitrogen and phosphorus collected on filters, using a semi-automatic wet-oxidation method. *Mar. Ecol. Prog. Ser.* **180**, 289–295 (1999).
66. EUMETSAT. *Recommendations for Sentinel-3 OLCI Ocean Colour Product Validations in Comparison With in Situ Measurements – Matchup Protocols*. [https://user.eumetsat.int/s3/eup-strap-media/Recommendations\\_for\\_Sentinel\\_3\\_OLCI\\_Ocean\\_Colour\\_product\\_validations\\_in\\_comparison\\_with\\_in\\_situ\\_measurements\\_Matchup\\_Protocols\\_V8\\_B\\_e6c62ce677.pdf](https://user.eumetsat.int/s3/eup-strap-media/Recommendations_for_Sentinel_3_OLCI_Ocean_Colour_product_validations_in_comparison_with_in_situ_measurements_Matchup_Protocols_V8_B_e6c62ce677.pdf) (2022).
67. Bailey, S. & Wang, M. Satellite aerosol optical thickness match-up procedures. *NA. SA Tech. Memorandum* **209982**, 70–72 (2001).
68. Kermack, K. A. & Haldane, J. B. S. Organic correlation and allometry. *Biometrika* **37**, 30–41 (1950).
69. York, D. Least-squares fitting of a straight line. *Can. J. Phys.* **44**, 1079–1086 (1966).
70. Guinehut, S., Dhomp, A. L., Larnicol, G. & Le Traon, P. Y. High resolution 3-D temperature and salinity fields derived from in situ and satellite observations. *Ocean Sci.* **8**, 845–857 (2012).
71. Mulet, S., Rio, M. H., Mignot, A., Guinehut, S. & Morrow, R. A new estimate of the global 3D geostrophic ocean circulation based on satellite data and in-situ measurements. *Deep-Sea Res. Part II Topical Stud. Oceanogr.* **77**, 70–81 (2012).
72. De Boyer Montégut, C., Madec, G., Fischer, A. S., Lazar, A. & Iudicone, D. Mixed layer depth over the global ocean: an examination of profile data and a profile-based climatology. *J. Geophys. Res. Oceans* **109**, C12003 (2004).
73. Beaulieu, C. et al. Factors challenging our ability to detect long-term trends in ocean chlorophyll. *Biogeosciences* **10**, 2711–2724 (2013).
74. Loisel, H. et al. Variability of suspended particulate matter concentration in coastal waters under the Mekong's influence from ocean color (MERIS) remote sensing over the last decade. *Remote Sens. Environ.* **150**, 218–230 (2014).
75. Delgado, A. L. et al. Seasonal and inter-annual analysis of chlorophyll-a and inherent optical properties from satellite observations in the inner and mid-shelves of the south of Buenos Aires Province (Argentina). *Remote Sens.* **7**, 11821–11847 (2015).
76. Delgado, A. L. et al. Patterns and trends in Chlorophyll-a concentration and phytoplankton phenology in the biogeographical regions of Southwestern Atlantic. *J. Geophys. Res. Oceans* **128**, e2023JC019865 (2023).
77. Hirsch, R. M., Slack, J. R. & Smith, R. A. Techniques of trend analysis for monthly water quality data. *Water Resour. Res.* **18**, 107–121 (1982).
78. Sen, P. K. Estimates of the regression coefficient based on Kendall's tau. *J. Am. Stat. Assoc.* **63**, 1379–1389 (1968).
79. Gilbert, R. O. *Statistical Methods For Environmental Pollution Monitoring* (John Wiley & Sons, 1987).
80. Allison, D. B., Stramski, D. & Mitchell, B. G. Seasonal and interannual variability of particulate organic carbon within the Southern Ocean from satellite ocean color observations. *J. Geophys. Res. Oceans* **115**, C06002 (2010).

## Acknowledgements

This work was supported by Centre National d'Etudes Spatiales in the frame of the COUP-PNP project (CNES/ TOSCA program), the postdoc funding for Alain Fumenia by the National Center for Space studies (CNES), the ANR CO2COAST project (ANR-20-CE01-0021 to H.L.), the graduate school IFSEA that benefits from a France grant (ANR-21-EXES-0011), and the Simons Foundation International-Life Sciences award (#00009452 to DMK). We are grateful to the scientists and crews involved in the OUTPACE (<https://doi.org/10.17600/15000900>) and TONGA (<https://doi.org/10.17600/18000884>) projects. We also thank the scientific teams involved in the HOT program at Station ALOHA. We thank all scientists and crew involved in fieldwork for their support and contributions to collection of data. We also thanks ACRI-ST for the production and the distribution of the satellite data used in this study. This study has been conducted using E.U. Copernicus Marine Service Information; <https://doi.org/10.48670/moi-00024>.

## Author contributions

A.F., H.L., and T.M. conceptualized the study. H.L. and A.F. contributed to the funding acquisition. H.L. contributed to the supervision of this study. T.M., S.B., M.B., A.M. and D.K. contributed to the acquisition of data. T.M., S.B., D.K., M.B. and A.M. performed the data curation. A.F. developed the computer code and supporting algorithms and performed visualization. A.F. and M.T.D. contributed to the application of statistical and computational techniques. A.F. contributed to the writing of the original draft preparation. A.F., H.L., T.M., D.K., V.V. and A.P. contributed to the investigation. A.F., H.L., T.M., D.K., V.V., and A.P. contributed to the interpretation of data. All authors contributed to the writing review and editing.

## Competing interests

The authors declare no competing interests.

## Additional information

**Supplementary information** The online version contains supplementary material available at <https://doi.org/10.1038/s41467-025-66743-3>.

**Correspondence** and requests for materials should be addressed to Alain Fumenia.

**Peer review information** *Nature Communications* thanks the anonymous reviewers for their contribution to the peer review of this work. A peer review file is available.

**Reprints and permissions information** is available at <http://www.nature.com/reprints>

**Publisher's note** Springer Nature remains neutral with regard to jurisdictional claims in published maps and institutional affiliations.

**Open Access** This article is licensed under a Creative Commons Attribution-NonCommercial-NoDerivatives 4.0 International License, which permits any non-commercial use, sharing, distribution and reproduction in any medium or format, as long as you give appropriate credit to the original author(s) and the source, provide a link to the Creative Commons licence, and indicate if you modified the licensed material. You do not have permission under this licence to share adapted material derived from this article or parts of it. The images or other third party material in this article are included in the article's Creative Commons licence, unless indicated otherwise in a credit line to the material. If material is not included in the article's Creative Commons licence and your intended use is not permitted by statutory regulation or exceeds the permitted use, you will need to obtain permission directly from the copyright holder. To view a copy of this licence, visit <http://creativecommons.org/licenses/by-nc-nd/4.0/>.

© The Author(s) 2025